Anomaly detection in adiabatic processes

Yu He
Department of Applied Physics
Stanford University, California 94305
Email: yuhe@stanford.edu

***Abstract*—Anomaly detection algorithm complements human surveillance in that it is capable of handling both very fast and large volume of observations. In this report, it is instead used to evaluate and detect anomalous behavior in video-recorded extremely slow processes, which can be as challenging for human perception. Morphological image processing techniques are used to separate the slowly evolving foreground from the background in a time sequence of images. By defining the corresponding metrics of the extracted foreground features and applying an Bayesian estimator to the sequence within a finite time window, the probability of the upcoming observation being an anomaly can be evaluated. Single crystal growth process with optical floating zone method is used as an example for application.**

I. Introduction

Anomaly detection has wide-spread use in common practices including surveillance video analysis, fraud detection, spacial disruption and vital sign monitoring [1]. However, some of the most labor intensive industry and state-of-the-art laboratory procedures have yet to fully utilize this application, sometimes due to slow and subtle accumulative nature of the processes. Among them, the monitoring of crop growth [2], food preservation, geological or ecological change [3] and single crystal growth [4] all share the commonality of a relatively static background and a slowly evolving foreground that carries the information of interest. Therefore, by analyzing the time lapse image sequence of the subject of interest, one can overcome the weakness of human perception on adiabatic changes, and promptly identify or even predict the appearance of an anomalous event.

In this report, we use a single crystal growth time lapse recorded over an effective duration of $\sim$300 hours on an optical floating zone furnace setup in Stanford Institute of Materials and Energy Sciences (SIMES), to demonstrate the viability of this frame-by-frame, morphological image processing based anomaly detection algorithm.

Optical floating zone method consists of a material rod (feed and seed rod), heating elements (lamp filament) and a set of focusing optics (gold plated mirrors), as indicated in Fig.1(a) [5]. During an actual growth, the thermal radiation of the filaments is tightly focused onto the polycrystalline material rod, thus creating a narrow section of molten zone up to 2500 degree Celsius. Then the material rod is moved downward adiabatically to have the material molten and recrystalize in a controlled fashion, releasing any potential structural strain and retaining impurities inside the liquid phase. When the molten zone finally travels to the top, the single crystal growth is then finished. This downshift process is typically extremely slow at 0.1mm/hour, and requires human attention through the entire process to monitor the stability of the molten zone, which is instrumental to achieve high quality final product. Fig.1(b-f) demonstrates various growth anomalies as a result of accumulative adiabatic change, captured by a fixed-position video camera.

II. Parametrization and extraction of the foreground

A typical molten zone contains the following key features that relate closely to its stability and health (Fig.2(a)).

- optical reflectivity (total brightness or intensity)
- zone volume (of the liquid phase, defined by the region between the upper and lower melt lines)
- center of mass (first moment)
- zone diameter (minima defined as the zone waist)
- eccentricity
- edge gradient/curvature

Each of these metrics represents a unique aspect of the molten zone. For instance, optical reflectivity is particularly sensitive to zone destruction and waist change; zone volume is sensitive to zone overflow, incongruent melting (unmelted solid breaks into molten zone) and zone shrinkage; center of mass (CoM) and edge gradient/curvature are sensitive to change in zone symmetry and zone wobbling.

In order to properly extract all the aforementioned parameters, separating the foreground molten zone from the background reflection of heating filaments is critical. In order to achieve such goal, the following steps are taken on frame-to-frame.

- find SURF key points for the background frame (frame 0, Fig.2(b)) and the incoming frame (Fig.2(c))
- match the SURF key points and compute the homographical transform matrix from the incoming frame to the background frame plane with RANSAC
- transform the incoming frame and align with the background frame (Fig.2(d))
- subtract the background frame from the incoming frame
- convert the subtracted RGB image to grayscale image (Fig.3(a))

Because the filament brightness changes from time to time, before the subtraction, the overall intensity of the incoming frame is also normalized to the background frame by matching the average intensity on the upperleft corner where no actively changing feature is present.

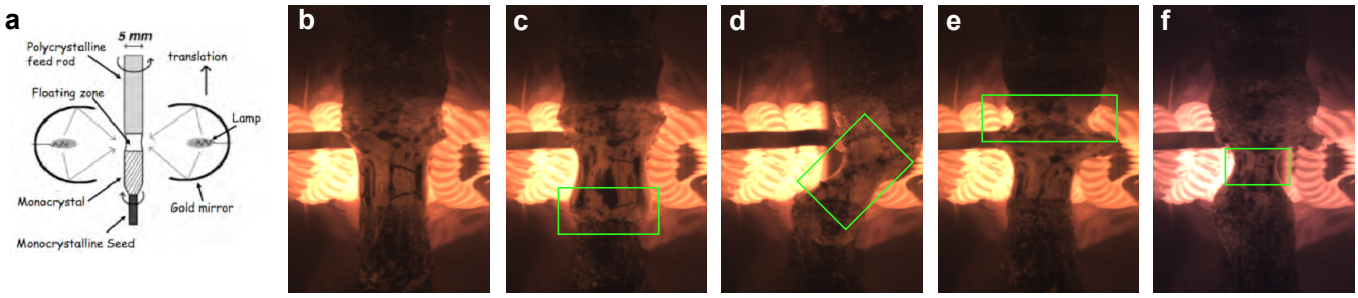

Fig. 1. Typical floating zone furnace setup and growth snapshots. (a) Illustration of the working principles of the floating zone method. (b) The molten zone in a normal growth of copper based high temperature superconductor. (c)-(f) Growths that show various zone instabilities: zone overflow, zone wobbling, incongruent melting, zone shrinking. The anomalous region is boxed in green.

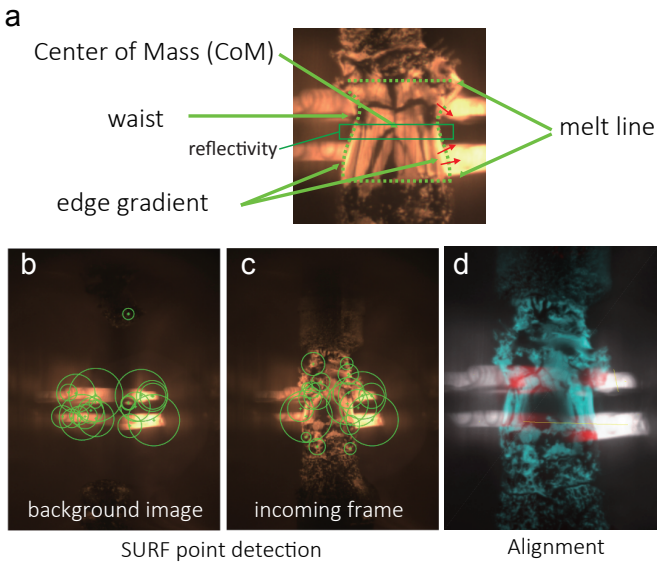

Fig. 2. Molten zone paramatrization and alignment. (a) Key parameters of the molten zone. (b) SURF key points on the background frame prior to the growth. (c) SURF key points for the actual growth frame. (d) Transform and align the background and actual crystal growth frame.

After the frame alignment, intensity normalization, subtraction and grayscale conversion, a series of morphological operations can be carried out to compute the binary mask of the molten zone. The main hurdle is the irregular dark reflection inside the zone, and the bright reflection close to the zone edge (all likely to mix with the background).

- dilate the grayscale image with a disk of radius 25px (Fig.3(a) $\rightarrow$ (b))
- binarize the frame with Ostu's method (Fig.3(b) $\rightarrow$ (c))
- flip foreground and background, label the foreground, and nullify all foreground that is not labeled at 0 (fill in the holes inside the molten zone) (Fig.3(c) $\rightarrow$ (d))
- flip the foreground and background again, and erode the foreground back down by the same size disk used in step 1 (Fig.3(d) $\rightarrow$ (e))
- use predefined melt line coordinate the crop out the non-liquid segments, and arrive at the binary mask for the molten zone (Fig.3(e) $\rightarrow$ (f)). Thanks to the tight focusing optics, the vertical position of the melt lines remain largely unchanged during typical growth
- use differentiation filter to compute the left and right edges of the molten zone (Fig.3(f) $\rightarrow$ (g))
- overlay the mask atop the actual frame to visually examine the agreement (Fig.3(g) $\rightarrow$ (h))

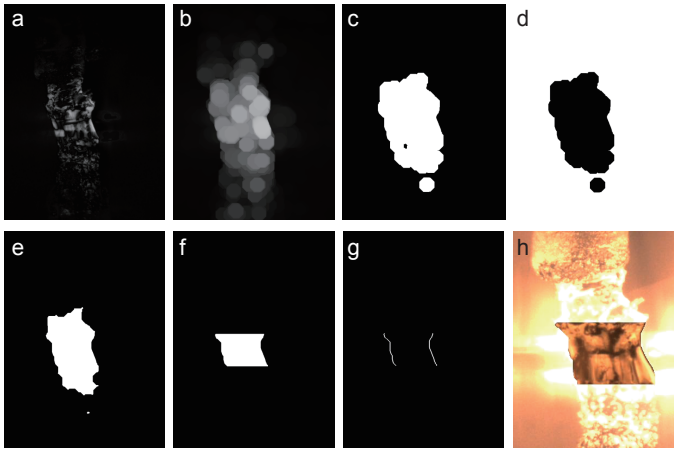

Fig. 3. Morphological image processing on a sample frame at +7.2 hours into the growth. Step by step illustration is stated in the text.

Hence, with the mask of the molten zone generated, several key metrics defined earlier can be computed. In this particular example, the following parameters are calculated:

- reflectivity - total pixel intensity count inside the green box area in Fig.2(a)
- zone volume - total area (zeroth moment) of the molten zone mask in Fig.3(f)
- center of mass (CoM) - first moment of the molten zone mask in Fig.3(f)
- zone diameter - distance from the left edge to the right edge of the molten zone as a function of the vertical position in Fig.3(f)
- edge gradient - left and right zone edge gradient as a function of the vertical position

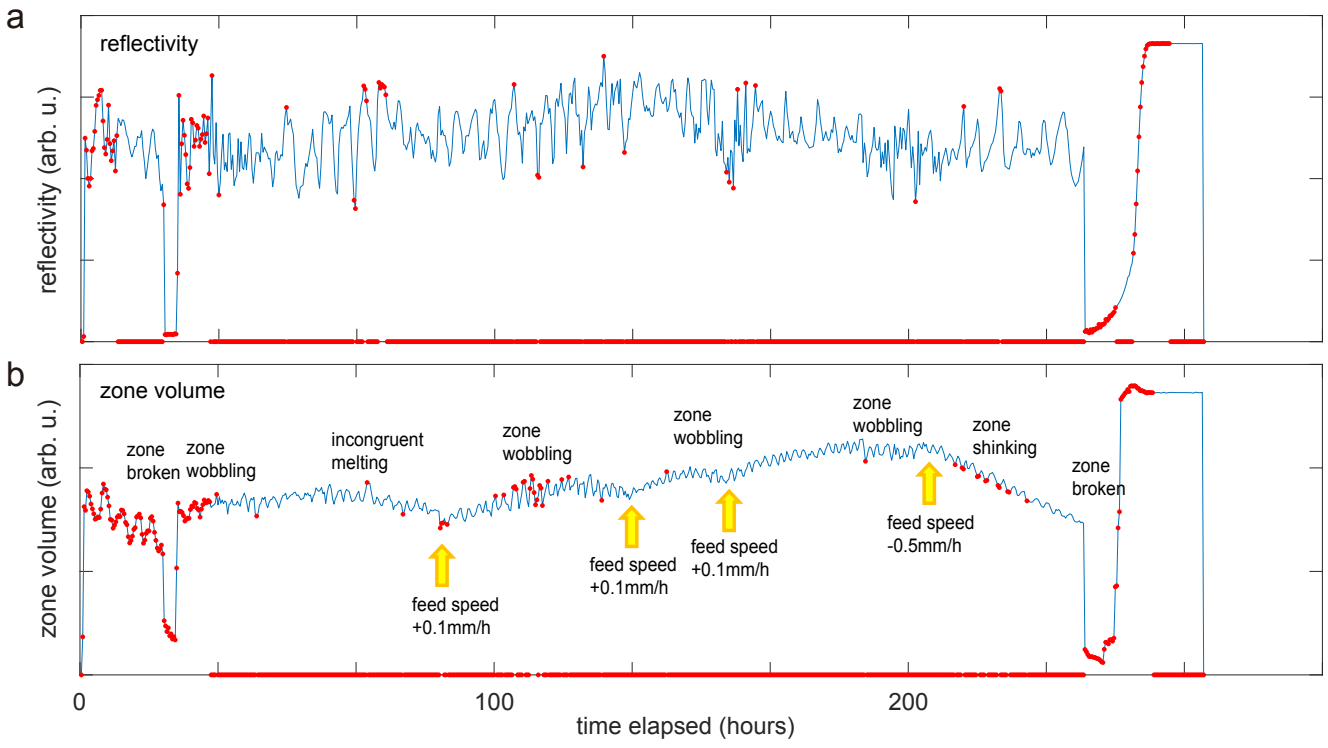

Fig. 4. Time dependent (a) reflectivity and (b) zone volume change in this particular growth. Red dots are the detected anomalies.

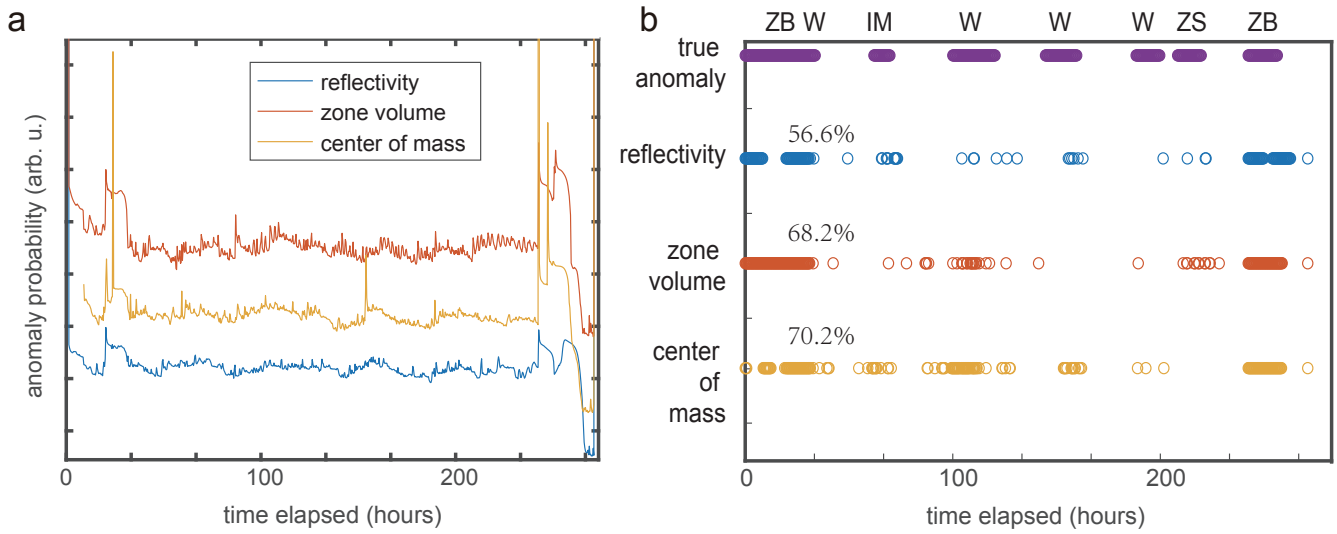

Fig. 5. Anomaly detection result from the three most representative parameters - reflectivity (blue), zone volume (orange) and center of mass (yellow). (a) Anomaly probability estimated over time. Curves are offset vertically for clarity. (b) Comparison of the anomaly detection results from the three channels to the true anomaly identified by human experimenter (purple). ZB - zone broken. W - zone wobbling. IM - incongruent melting. ZS - zone shrinking.

III. Anomaly Detection

Once the zone parameters are extracted per frame, real time time sequence analysis can be performed to detect the anomaly or even predict the anomaly by analyzing the sign of accumulative change. In principle, more complicated Kalman gain and control input can be included. But just to demonstrate the principle, Fig.4 shows the anomaly detection result (red dots) based on a simple constant bayesian estimator. The demonstration here is a time lapse footage sampled every 24 minutes over the course of $\sim$ 300 hours. The following procedures are taken to detect the anomaly:

- define a moving average time window that reflects the

intrinsic time scale of the process (10 hours, or 25 frames in this case)

- compute the mean and standard deviation of the parameter over the define time window before the current time
- compute the probability of the incoming parameter at current time based on the t-distribution estimated from the previous step
- if the probability falls below a threshold, classify the current frame as an anomaly
- take action (might either send out an alert email, or execute direct control on the hardware motor)

Fig.4 demonstrates the time dependent reflectivity (a) and volume (b) change over the entire course. The fast periodic wiggles are results of the sample aliasing from the frame capturing process (the material rods are rotating 3.2 revolutions per minute). Regardless, the estimator is able to tolerate the aliasing artifact and pick up most expected anomalies (labeled by the red dots). It can also be seen that the detection may also serve as a guide for preventing catastrophic event (zone breaking). For example, in Fig.4(b), the zone volume sequence reports repeated anomalies right before both two zone breaking events usually more than 10 hours ahead of time, which can earn experimenters precious time to perform correction after being alerted.

Another handy feature is the indication of tiny (but accumulative) growth parameter changes. The yellow arrows in Fig.4(b) indicates the time when the experimenter manually increased the material rod feed speed by just 0.1mm/h, which is usually hardly perceptible by human in real time. What's more intriguing is the observation of the three repeated patterns of 'speed-increase $\rightarrow$ zone-wobbling ', which reveals the unforeseen underlying causality - with increased material feed speed, heating power requirement becomes insufficient, causing zone crystallization in the center thus the wobbling (forced breaking of the zone center crystallization due to rotation).

TABLE I
DETECTION RATE COMPARISON.

	reflectivity	zone volume	center of mass	total
detection rate	56.6%	68.2%	70.2%	88.1%

To quantify the anomaly detection accuracy, the detection results are compared with after-fact human-identified anomalies (true anomaly). Fig.5(a) plots the anomaly probability for three channels (log plot, curves offset vertically for clarity). After setting their respective anomaly acceptance thresholds, the positive anomaly detection results are listed in Fig.5(b) as a function of elapsed time. The purple line on top is the true anomaly. It suggests that indeed, the canter of mass (yellow) captures more anomalies from zone wobbling events, and the reflectivity (blue) is sensitive to more severe events like disruption in the zone center (zone broken). The zone volume metric (orange) appears to be a balanced compromise of the other two metrics.

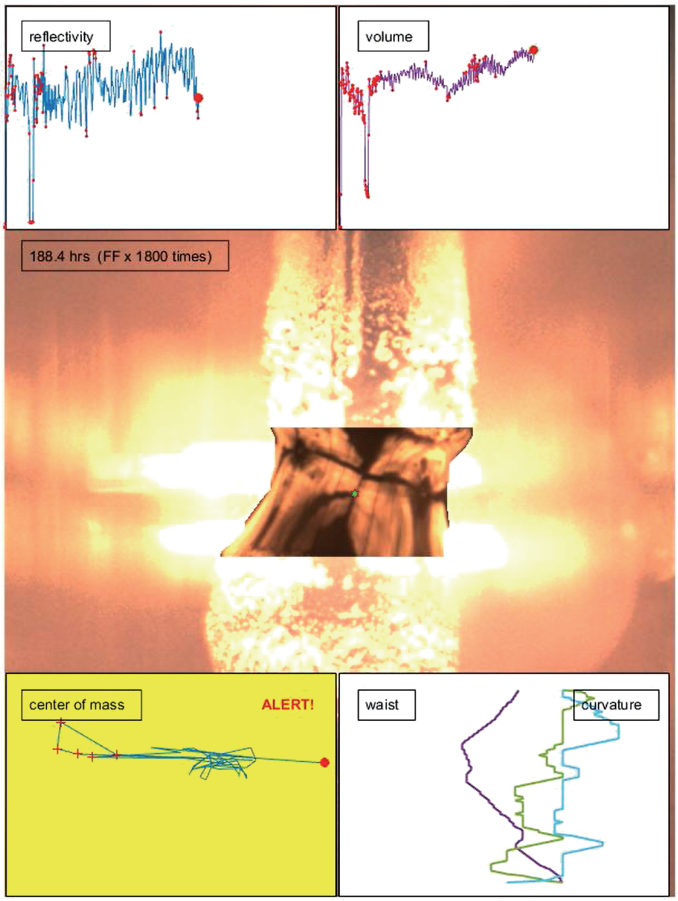

Fig. 6. Operation panel in live action.

Assuming each positive detection represents a time window same size as what the previous detection algorithm designated (see section III, 5 hours each side in this case), the overlap between the positive detection (from each channel) and the true anomaly can be computed. Similarly, the combined detection rate can also be computed by taking OR operation among the three channels first. The results are summarized in the following TABLE I.

IV. Demonstration and Discussion

Fig.6 demonstrates the program processing the time lapse frames in real time. When there is an anomaly detected, the corresponding channel will flick yellow. The center of mass channel only displays the 50 most recent frames, where red crosses denotes anomalies. The lower right corner also plots the vertical profile of the zone diameter and left/right edge gradient. In this particular frame, the zone is in a wobbling anomaly, and shows clear eccentric shape. In this scenario, the left (green) and right (cyan) edge gradients will display clear deviation from each other, signaling asymmetry in the zone shape. These features can be utilized in the future to facilitate further improved accuracy in depicting the zone characters and instabilities.

While the crystal growth is used as the example in the report, this technique can be generalized to many other similar applications involving adiabatically evolving objects of interest. For example, food preservation, climate change, volcanic activity watch and crop growth monitoring may be promising application areas.

ACKNOWLEDGMENT

The author wishes to thank Prof. Gordon Wetzstein and Junfeng He for critical inputs for this project, and Prof. Zhi-Xun Shen for his generous support in the SIMES laboratory. The optical floating zone furnace and material synthesis setup are supported by US Department of Energy, Office of Sciences.

REFERENCES

[1] Chandola, V., Banerjee and A., Kumar, V. (2009). Anomaly detection: A survey. ACM computing surveys (CSUR), 41(3), 15.

[2] Ji-Hua, Meng, Wu Bing-Fang, and Li Qiang-Zi. A Global Crop Growth Monitoring System Based on Remote Sensing. 2006 IEEE International Symposium on Geoscience and Remote Sensing, pp. 2277-2280. Ieee, 2006.

[3] Bettencourt, Lus MA, Aric A. Hagberg, and Levi B. Larkey. Separating the wheat from the chaff: practical anomaly detection schemes in ecological applications of distributed sensor networks. International Conference on Distributed Computing in Sensor Systems, pp. 223-239. Springer Berlin Heidelberg, 2007.

[4] Y. Sun and H. Li, Diameter Detection for Crystals Growth Based on Image Processing, 2014 Sixth International Conference on Intelligent Human-Machine Systems and Cybernetics, Hangzhou, 2014, pp. 64-66. doi: 10.1109/IHMSC.2014.118

[5] Bertrand Poumellec, Matthieu Lancry, Santhi Ani-Joseph, Guy Dhalenne and Romuald Saint Martin (2012). Elaboration of a Specific Class of Metamaterial: Glass in Single Crystal, Crystallization and Materials Science of Modern Artificial and Natural Crystals, Dr. Elena Borisenko (Ed.), InTech, DOI: 10.5772/30385.